JOURNAL OF GEOPHYSICAL RESEARCH, VOL. 112, G04S36, doi:10.1029/2007JG000452, 2007

A glacier respires: Quantifying the distribution and respiration CO_2 flux of cryoconite across an entire Arctic supraglacial ecosystem

Andy Hodson,[1] Alexandre M. Anesio,[2,3] Felix Ng,[1] Rory Watson,[4] Joe Quirk,[1] Tristram Irvine-Fynn,[1] Adrian Dye,[1] Chris Clark,[1] Patrick McCloy,[4] Jack Kohler,[5] and Birgit Sattler[6]

Received 23 March 2007; revised 28 August 2007; accepted 3 October 2007; published 28 December 2007.

[1] This paper quantifies the mass distribution of cryoconite at the glacier scale using photographic surveys conducted either at ground level, or at 20 m elevation using a novel uninhabited aerial vehicle (UAV). Image acquisition allowed three key deposits to be quantified: cryoconite holes, cryoconite in streams (''stream cryoconite''), and dispersed cryoconite granules (detectable only in the ground-based images). Cryoconite was found all over the snow-free parts of the glacier in one or more of these forms, covering about 0.42% (4600 kg km^{-2} dry weight) as holes and stream cryoconite deposits (>0.25 cm^2 and thus visible in the UAV images), or 1% (10600 kg km^{-2}) when smaller dispersed granules were included (using the ground images). No spatial patterns in the distribution of cryoconite cover were apparent, although cryoconite holes were far more common than stream cryoconite at high altitude due to lower melt rates. Measurements of respiration and bacterial carbon production estimated from in situ incubations of cryoconite–water mixtures indicated rates of 1.174 ± 0.182 (1 standard deviation) and 0.040 ± 0.019 μg C g^{-1} h^{-1}, respectively. The respiration measurements then yielded glacier-wide CO_2 fluxes for 1998 and 2000 of 6.3 and 5.1 kg C km^{-2} a^{-1} when the loci and duration of activity were defined using the UAV images and a degree day model, respectively. These fluxes increased to 14 and 12 kg C km^{-2} a^{-1} when the dispersed cryoconite detected in the ground-based images were also considered. The measurements therefore show that cryoconite ecosystems clearly have the capacity to impact upon carbon cycling in glacial environments.

Citation: Hodson, A., et al. (2007), A glacier respires: Quantifying the distribution and respiration CO_2 flux of cryoconite across an entire Arctic supraglacial ecosystem, *J. Geophys. Res.*, *112*, G04S36, doi:10.1029/2007JG000452.

1. Introduction

[2] Cryoconite is a 19th century term for the granular, organic-rich debris found upon glaciers and sea ice. It plays a vital role in the biogeochemistry and ecology of ice, especially in glacial environments characterized by low accumulation area ratios and prolonged surface ice ablation during the summer [see *Hodson et al.*, 2007]. In Svalbard, cryoconite mostly consists of fungal, algal and bacterial cells with a high incidence of viral infection [*Anesio et al.*, 2007; *Säwström et al.*, 2007]. These consortia are surprisingly active and therefore impact significantly upon the abundance and phase distribution of nutrients liberated by the melt process [*Hodson et al.*, 2005a], as has been inferred elsewhere [e.g., *Tranter et al.*, 2004]. Activity occurs in a number of habitats – none of which have been adequately quantified at the system (glacier) scale, anywhere in the cryosphere. The habitats include cryoconite holes, cryoconite in streams (''stream cryoconite'') and dispersed cryoconite, draped as granules over the glacier's ice surface (Figure 1). After the removal of the snowpack, the cyclic redistribution of cryoconite granules from one habitat to another almost certainly takes place, because new stream cryoconite deposits form after melt out (or stream invasion) of cryoconite holes [cf. *Takeuchi et al.*, 2000]. Thereafter, the authors' observations from Svalbard suggest that new cryoconite holes may then form from the larger stream cryoconite deposits, while smaller dispersed deposits often become ''stranded'' (usually due to changes in the near-surface hydrology of the glacier surface) before being captured once more by surface streams.

[1]Department of Geography, University of Sheffield, Sheffield, UK.
[2]Institute of Biological Sciences, University of Wales, Aberystwyth, UK.
[3]Now at Bristol Glaciology Centre, School of Geographical Sciences, University of Bristol, Bristol, UK.
[4]HighSpy, Elstead, UK.
[5]Norsk Polarinstitutt, Polar Environmental Center, Tromsø, Norway.
[6]Institute of Ecology, University of Innsbruck, Innsbruck, Austria.

0148-0227/07/2007JG000452$09.00

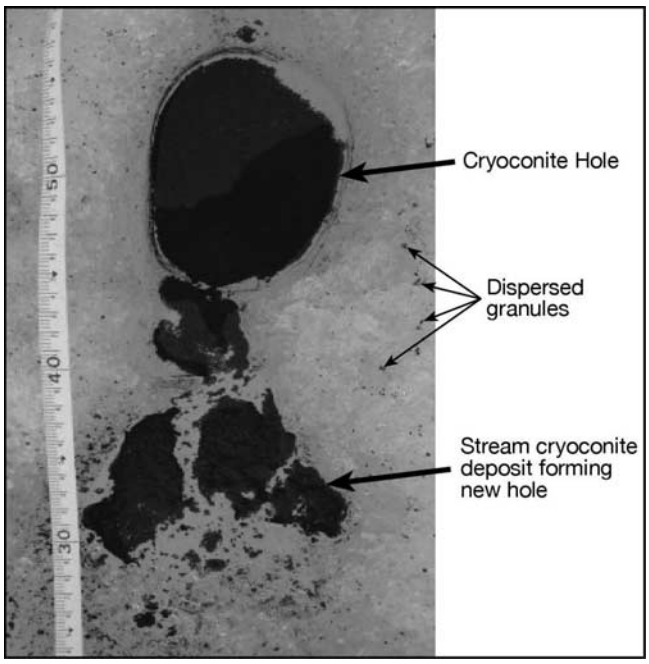

Figure 1. Cryoconite holes, stream cryoconite and dispersed cryoconite.

[3] At Midtre Lovénbreen (in Svalbard), studies of microbial ecology in cryoconite have been limited to a few holes. For example, *Kaštovská et al.* [2005], *Säwström et al.* [2002, 2007], *Mindl et al.* [2007], and *Anesio et al.* [2007] describe the cyanobacteria, algae, other bacteria and viruses that are present. The cyanobacteria and other primary producers support remarkably significant rates of photosynthesis ($\sim$1–160 μg C L^{-1} h^{-1} according to *Säwström et al.* [2002]; or 1 to 100 μg C g^{-1} h^{-1} according to B. Sattler (unpublished data, 2006)). These in situ estimates of primary production are among the first of their kind and demonstrate the need to reassess glacier and ice sheet surfaces as active biological systems in their own right. Measurements of secondary production are even more scarce, and at Midtre Lovénbreen they have until now been restricted to laboratory-based determinations of community respiration at far from natural environmental conditions [see *Kaštovská et al.*, 2005].

[4] Many more studies of the rates of microbial activity in cryoconite and the formation, longevity and destruction of their habitats are required before carbon cycling within supraglacial ecosystems will be fully understood. The present paper therefore addresses this shortcoming directly by presenting the first quantification of glacier-wide microbial activity (in this case, respiration) within cryoconite habitats following their exposure by snowpack retreat during the summer. In so doing, we quantify the distribution of cryoconite across the entire glacier surface for the first time after applying a novel surveillance method using a remote control aircraft.

2. Field Site and Methods

[5] M. Lovénbreen is a well-known polythermal valley glacier in West Spitsbergen, Svalbard. It has been subject to glacier mass balance monitoring since the late 1960s [*Hagen et al.*, 2003], during which only 4 a of positive mass balance have been recorded. Thus high end-of-summer snow lines are common here and it is not unusual for the snow covered area at the end of summer to be <10% of the glacier surface (the average since 1969 is 35% (J. Kohler, unpublished data, 2005)). The surface energy balance conditions for ablation upon the glacier are described by *Hodson et al.* [2005b]. These data sets show that surface melting of over 2 m a^{-1} is possible in the lower ablation area. Like many other glaciers, the melting is dominated by incident radiation (74–100% of the total summer melt depending upon the elevation), allowing cryoconite holes to form all over the snow-free glacier surface. Typically, the holes are $\sim$8 cm deep and 0.6–35 cm diameter [*Hodson et al.*, 2007] which corresponds to $\sim$0.1–1000 g of debris (see Figure 3). However, the glacier's northerly aspect, frequent supraglacial stream migration and periodic exposure to energy advection from warm air masses, often result in the complete melt out of holes across much of the glacier. This is particularly so in late summer, when low Sun angles yet stable, high air temperatures promote reworking of the cryoconite, delivering it to the streams and forming irregular stream cryoconite deposits (Figure 1). An advantage of these conditions is that the cryoconite can be easily discerned from aerial photographs. The collection, processing and calibration of such images are therefore described below.

2.1. Aerial Surveillance in 2005

[6] During August 2005, a remote-controlled helicopter or "uninhabited aerial vehicle" (hereafter the "UAV") was used in conjunction with a gyroscopically mounted Canon Eos 300D digital camera for 6.29 Mpixel image capture from a flying altitude of 20 m. The UAV, a 323 Heliball (http://www.highspy.co.uk/, Figure 2) is ideal for reconnaissance because a radio link ensures that a ground-based operator can control and optimize image acquisition during flight and, unlike fixed-wing UAVs, while hovering. The UAV therefore provided an excellent basis for capturing images of cryoconite from a much larger expanse of the glacier than would have been possible using ground-based surveillance. Seven transects of $\sim$600–800 m were flown across the glacier between 150 m and 375 m altitude (Figure 4), providing representative images of the entire snow-free surface of the glacier except for elevations below 100 m and above 450 m. Here, steep slopes and either snow or moraine cover prevented accurate surveys. The image footprint was ca. 154 m^2 and no radial distortion was discernable from images that contained targets of known dimensions. Processing was undertaken to identify cryoconite deposits down to single pixel resolution (0.245 cm^2). In all, an average of 25 acceptable images were processed from each transect (see Figure 4). While the UAV reconnaissance clearly offered a broad spatial coverage of the glacier, a weakness of the method is that dispersed cryoconite could not be resolved in the images captured. These individual granules were too small (typically 1–4 mm diameter) and so their distribution was assessed using ground-based image acquisition (see below).

[7] The processing of the UAV images involved a supervised classification procedure on an image by image basis

Figure 2. HighSpy UAV showing the gyroscopically mounted camera at the front of the craft.

using Erdas Imagine 8.7. This easily resolved the presence of dark cryoconite against bright ice, provided that images with large moraine clasts were not processed (e.g., in the lower 100 m of the glacier). After processing, all the streams in each image were manually selected as areas of interest in order to separate the cryoconite deposits into either stream cryoconite or cryoconite holes. In a few cases the position of streams was not obvious in the classified images and so stream cryoconite was identified visually according to the presence of meandering or linear patterns of deposition.

2.2. Ground-Based Surveillance in 2006

[8] The purpose of the 2006 field program was to use ground-based photogrammetry of 0.25 m^2 quadrats in order (1) to survey parts of the Midtre Lovénbreen surface that were unsuitable for the UAV (steep slopes and the lower glacier below 150 m elevation) and (2) to assess the proportion of total cryoconite cover that was dispersed as single or small clusters of granules and thus beyond the limits of the UAV camera's resolution. In both cases, images were captured using a Fuji FinePix in a macro lens mode at 1.5 m above the ice surface with a 2 Mpixel resolution. Images were taken of a 0.5 $\times$ 0.5 m quadrat and were free of detectable radial distortion. In excess of 1000 images were collected in this manner from 10 sites (see Figure 4). At each site images were taken along intersecting 10 m transects. Processing of the images followed the same procedure as above. Figure 4 shows that the elevation range of the ground-based surveillance was 100 m to 430 m altitude and thus greater than that achieved with the UAV. However, due to differences in the August snow lines of 2005 and 2006, we were unable to assess cryoconite cover using ground-based images from the glacier center line above 340 m (i.e., the main trunk of the glacier).

2.3. Ground Truthing

[9] Ground truthing was undertaken in both years in order to transform the areal coverage of the cryoconite to an estimate of the dry mass. Cryoconite deposits in holes and streams were therefore photographed, measured and then removed using a 100 mL syringe, filtered through a 0.45 μm filter and oven dried at 30°C before weighing. The relationship between the measured area (A, in cm^2) and dry mass for cryoconite holes and stream cryoconite deposits ($M_c^{h,s}$ in g) was then found to be

$$M_c^{h,s} = 0.126A - 0.250 \quad (1)$$

The coefficient of determination was 99.8%, the number of observations was 35, and the standard error of the slope just 0.005. Unlike the slope, the intercept was not significantly different from zero.

[10] In the case of the dispersed cryoconite, feature area could not be measured and so surface ice samples with dispersed cryoconite deposits were removed from the glacier using an ice axe and photographed upon a white sheet. The total cryoconite mass (M_c^{disp}) was estimated from the number of pixels classified as cryoconite, resulting in

$$M_c^{disp} = 0.122A_p - 0.438 \quad (2)$$

where A_p is the area in cm^2 of the pixels classified as cryoconite (each pixel being 0.0018 cm^2), r^2 was 0.91, and

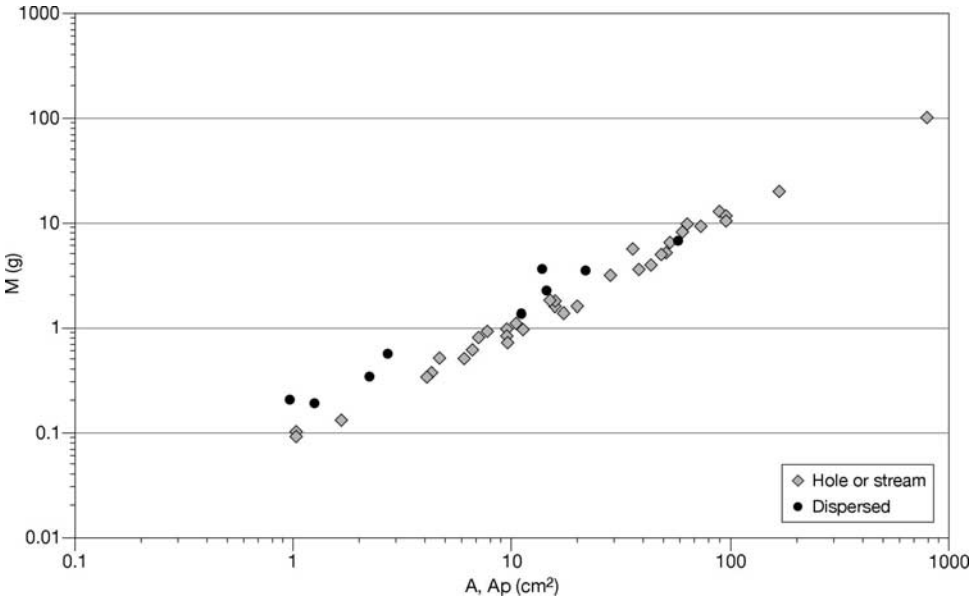

Figure 3. Relationship between the area of cryoconite deposit and the dry mass present.

the slope standard error 0.014. Again, the intercept was not significantly different from zero.

[11] Figure 3 shows the relationships depicted by equations 1 and 2. The close agreement between the two data populations (especially where $A > 3$ cm^2) demonstrates a similarity between the measured area (A in equation (1)) and the derived pixel area (A_p in equation (2)). The similar, linear relationships also reflect the tendency for all types of cryoconite deposit to have a uniform thickness equivalent to a single layer of granules. With this being the case, the mass of cryoconite in each image (M_c) was estimated directly from the total pixel area A_p (in cm^2) classified as cryoconite using

$$M_c = 0.124 A_p \quad (3)$$

The coefficient 0.124 (standard error ±0.005 g cm^{-2}) is the mean of the slopes of equations (1) and (2).

2.4. In Situ Bacterial Production and Community Respiration

[12] In this study, leucine incorporation was used to indicate carbon incorporation through the heterotrophic bacterial community, while oxygen consumption was used to quantify the carbon respired by both by prokaryotic and eukaryotic communities. Triplicate incubations were conducted across the glacier ablation area at elevations between 100 and 400 m altitude. Samples included stream cryoconite deposits (three sites), hydrologically isolated cryoconite holes (three sites) and cryoconite holes that showed a clearly discernable throughflow of surface meltwater (four sites). At each site, bacterial production in the debris and water were estimated from the incorporation of ^{3}H-leucine using the microcentrifuge method modified from *Kirchman* [2001] and the filtration method according to *Bell* [1993], respectively. Incubation of both water and sediment samples took place at in situ temperatures upon the glacier surface. The ^{3}H-leucine was added to a final concentration of 40 nM and 100 nM for water and sediment samples, respectively. For water samples, triplicate 20 mL samples and two control samples were incubated for 3 h and the incubation was terminated by the addition of "TCA" (trichloroacetic acid at 5% final concentration). Samples were filtered through 0.22 μm cellulose acetate filters and washed with three volumes (5 mL) of 5% ice cold TCA. Thereafter, the filter was dissolved with 1 mL ethylacetate, 10 mL of scintillation fluid and counts conducted with a Beckman LS6500 scintillation counter. For debris samples, triplicate 1.7 mL samples and two control samples, collected with an automatic pipette with a broad end tip in order to collect sediment material plus water, were added into 2 mL microcentrifuge tubes. Samples were incubated for 3 h. After incubation, 90 μL of 100% TCA were added to the samples. The tubes were then centrifuged at 16,000 g for 10 min, following washing, centrifugation and aspiration of the supernatant with 5% TCA and 80% ethanol. The final supernatant was aspirated, and the remaining sediment was weighted for the calculation of bacterial production on a mass basis. Finally, 1 mL of scintillation cocktail (Ecoscint) was added and the samples counted by liquid scintillation. Although the method for measuring bacteria production in the sediments produced substantially higher blanks (i.e., higher amounts of residual nonincorporated radioisotope in the sample) than in water samples, the radioisotope activity of the control samples was less than 5% of the measured activity in noncontrol samples. Leucine incorporation rates were then transformed into bacterial carbon production according to *Smith and Azam* [1992]. It should be noted that the leucine method may account for both heterotrophic and cyanobacteria production, while community respiration, described below, incorporates respiration from all (eukaryotic + prokaryotic) organisms.

[13] Community respiration was monitored by measurements of dissolved oxygen consumption using a dissolved oxygen meter (YSI 550a) with a 0.01 mg L^{-1} resolution. Water (with and without debris) was taken from the cry-

Table 1. Respiration Fluxes by Elevation and for the Entire Glacier During the 1998 and 2000 Summers[a]

Elevation Range, m	M_C, g × 10^6	Ice Area, km^2	Bw 1998, m	Bw 2000, m	1998 Season, d	2000 Season, d	C_R 1998, kg C a^{-1}	C_R 2000, kg C a^{-1}
0–75	0.54	0.12	0.18	0.17	74	66	1.14 ± 0.43	1.00 ± 0.38
76–125	1.31	0.29	0.26	0.23	68	60	2.53 ± 0.96	2.21 ± 0.84
126–175	1.58	0.35	0.32	0.27	64	55	2.85 ± 1.08	2.46 ± 0.93
176–225	1.44	0.41	0.38	0.32	59	50	2.40 ± 1.01	2.04 ± 0.86
226–250	1.39	0.24	0.42	0.35	56	47	2.18 ± 0.92	1.84 ± 0.77
251–275	2.52	0.35	0.45	0.37	53	44	3.78 ± 1.32	3.15 ± 1.10
275–325	3.10	0.67	0.5	0.41	50	41	4.35 ± 1.44	3.58 ± 1.19
326–360	3.31	0.5	0.55	0.45	46	38	4.33 ± 1.34	3.50 ± 1.08
361–400	2.07	0.52	0.59	0.48	42	33	2.48 ± 1.10	1.95 ± 0.87
401–450	2.91	0.73	0.65	0.52	38	30	3.11 ± 1.38	2.46 ± 1.09
451–550	3.39	0.85	0.74	0.59	31	23	2.96 ± 1.31	2.19 ± 0.97
551–600	0.00	0.09	0.8	0.74	0	0	0	0
601–650	0.00	0.02	0.89	0.76	0	0	0	0
651–700	0	0	0.95	0.81	0	0	0	0
Cryoconite holes and stream cryoconite (UAV data)								
Totals, kg km^{-2} a^{-1}	23.6	5.14					32.1 ± 3.82	26.4 ± 3.12
Totals, kg km^{-2} a^{-1}	4590						6.25 ± 0.74	5.13 ± 0.61
Including dispersed[b]								
Total, kg km^{-2} a^{-1}	54.6						74.1 ± 11.1	60.9 + 9.08
Total, kg km^{-2} a^{-1}	10600						4.4 ± 2.16	11.8 ± 1.77

[a]Respiration fluxes are C_R ± standard errors, Bw is the winter snow accumulation in water equivalent (after J. Kohler, unpublished data, 2005).
[b]Data here have been multiplied by 2.306 in order to account for dispersed cryoconite granules.

oconite holes with an epidermic syringe and distributed into triplicate Pyrex glass bottles (50 mL) with ground glass stoppers. Initial dissolved oxygen concentration was measured immediately and the bottle was incubated in the dark at in situ temperature with no head space. New oxygen measurements were conducted after 24 h and the oxygen consumption was converted to carbon, using a respiratory quotient of 1. The debris in bottles containing debris and water was dried and weighted for the calculation of community respiration on a mass basis. It is appreciated that variations in the respiratory quotient were possible, but there is simply no information available to assess its likelihood and magnitude in glacial ecosystems. However, the use of a fixed value is partly justified by the negligible variations in cryoconite temperature across the snow-free parts of the glacier during summer.

2.5. Glacier-Wide Mass Distribution and Respiration Fluxes

[14] The purpose of this section is to demonstrate how a crude, glacier-scale estimate of cryoconite debris mass and associated respiration CO_2 flux can be derived by coupling the processed images and the in situ community respiration rate data.

[15] Our UAV transects fell within discrete elevation intervals (EIs) of between 25 and 50 m range, whose glacier surface area and typical winter snowpack depths (using 1998 and 2000 data) are reported in Table 1. The UAV transects were used to estimate the mass of cryoconite present in these EIs (i.e., $M^i_{C\mathrm{tot}}$ in g) using:

$$M^i_{Ctot} = k^i \overline{M}^i_C \tag{4}$$

where k^j is the ratio of the glacier area in the ith EI to the image footprint area (which was identical for all UAV images) and $\overline{M}^i_C$ is the average cryoconite mass from all images processed within the transect (each estimated using equation (3)). Since we had no UAV images for EIs below 125 m (8% of the glacier area), we used $\overline{M}^i_C$ from the next up-slope EI (i.e., 125–175 m). Similarly, for EIs above 400 m elevation (33% of the glacier surface area, but between 0 and 31% of its ablation area), we used $\overline{M}_C$ from the 361–400 m EI. However, beyond 550 m (just 2.1% of the glacier surface area), no cryoconite was assumed to be biologically active on account of the presence of perennial snow cover, steep glacier surface slopes and low summer temperatures.

[16] Following estimation of M^i_{Ctot}, the respiration fluxes from the glacier's elevation zones were calculated thus:

$$C^i_R = M^i_{Ctot} R d \tag{5}$$

where C^i_R is the carbon flux due to microbial respiration for the ith elevation zone (kg C a^{-1}); R is the average respiration rate per unit mass from Table 2 (1.17 μg C g^{-1} d^{-1}, standard error 0.056 μg C g^{-1} d^{-1}) and d is the duration of snow-free melting conditions (in days) within each elevation zone, estimated using a simple degree day index model that has been validated against energy balance and ablation measurements [*Hodson et al.*, 2005b; T. Irvine-Fynn, unpublished data, 2005]. The same daily respiration rate was used all over the glacier because our measurements showed no systematic change with elevation. However, it is appreciated that a good deal more measurements are required before a homogeneous respiration rate can be fully justified. The glacier-wide estimation of the respiration flux was therefore produced by simple aggregation of the EI respiration totals:

$$C_R = \sum_{i=1}^{i=N} C^i_R \tag{6}$$

Table 2. Summary Statistics of Bacterial Activity and Respiration[a]

	Bacterial Production				Community Respiration			
	Minimum	Maximum	Mean	SD	Minimum	Maximum	Mean	SD
Activity in water, μg C L^{-1} h^{-1}	0.0035	0.0078	0.0053	0.0017	1.1	2.6	1.5	0.78
Activity in debris, μg C L^{-1} h^{-1}	0.307	0.953	0.545	0.230	50.5	107.2	65.2	23.0
Activity in debris, μg C g^{-1} h^{-1}	0.016	0.051	0.040	0.019	0.91	1.44	1.17	0.180
Percent of total activity in the debris	99%				98%			
Number of habitats measured	8				10			

[a]As deduced from the radiolabel incorporation and dissolved oxygen consumption methods, respectively. Values are the average of three replicates in each case. SD is the standard deviation.

No respiration was assumed to take place beneath snow covered parts of the glacier and so we have effectively assumed that the onset of melting conditions and bacterial activity in a given EI is coincident with the removal of its snow cover. In reality, the onset of activity is probably slightly earlier, depending upon the thickness of superimposed ice layers above the glacier surface and the physical properties of the snowpack. The potential importance of subsnowpack respiration in cryoconite habitats is therefore considered in the discussion.

[17] The results, based upon well-defined snow line retreat patterns and appropriate meteorological data from the summers of 1998 and 2000 are shown in Table 1. Indicative estimates of uncertainty in the fluxes are also included, derived from statistical treatment of the standard error of all measured quantities in equations (3)–(6) [after *Taylor*, 1982].

2.6. Respiration by Dispersed Cryoconite

[18] The above calculations were initially undertaken using just the UAV-derived estimate of $M^i_{C\mathrm{tot}}$ and thus ignored habitats smaller than 0.25 cm^2. However, since the smaller, dispersed cryoconite granules also lay upon melting ice, it is conceivable that respiration took place at similar rates to those observed in the incubations. The average ratio of cryoconite cover estimated from the ground images to that from the UAV images at the same sites (see Figure 4) was therefore used to scale $M^i_{C\mathrm{tot}}$. The average of the ratios was 2.31 (standard error 0.55) and Table 1 shows

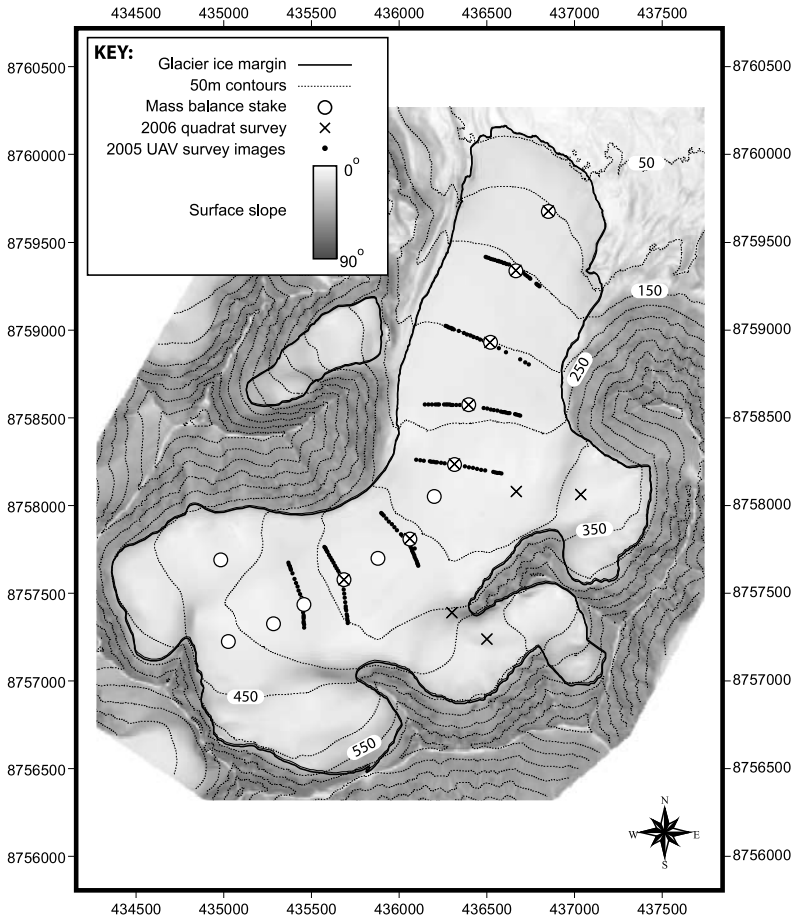

Figure 4. Samples sites upon Midtre Lovénbreen. The glacier is projected in UTM coordinates.

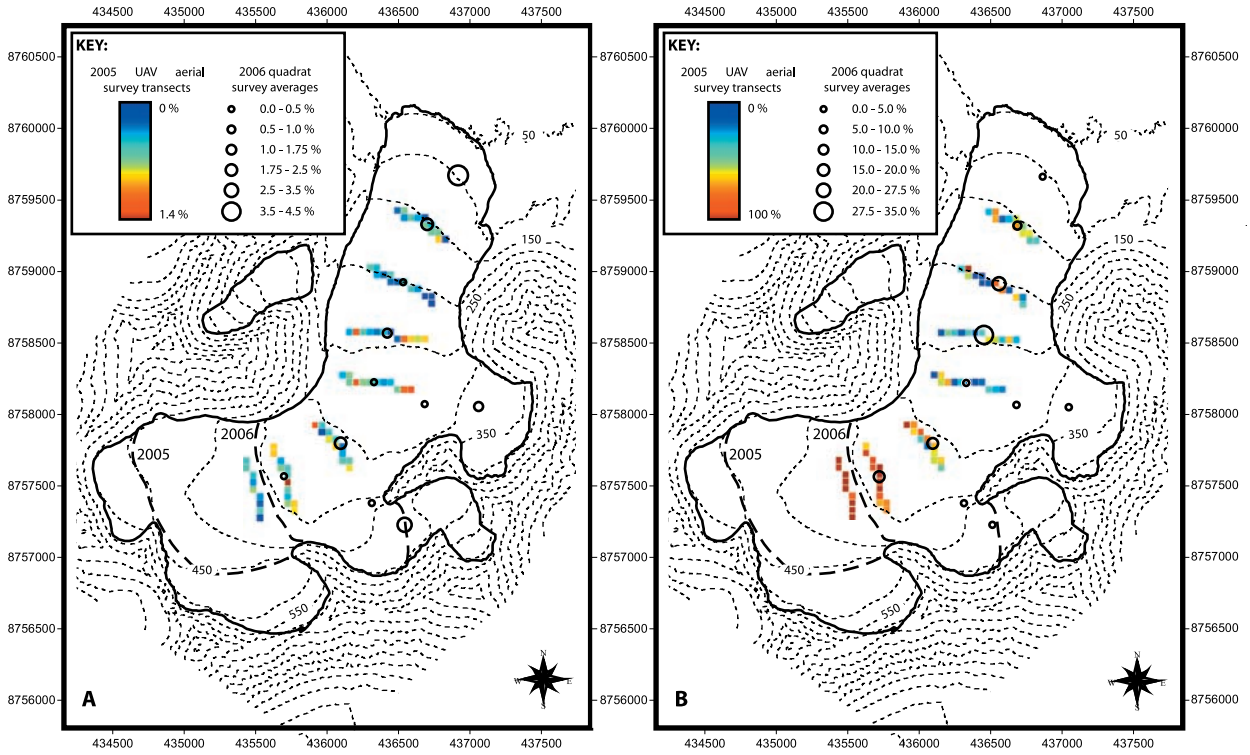

Figure 5. (a) Cryoconite cover expressed as a percentage of the glacier surface area. (b) Proportion of cryoconite cover within cryoconite holes. In both Figures 5a and 5b, the UAV data have been averaged to produce a clearer 50 × 50 m grid, and open circles have been used to represent averages of the ground-based images.

its impact as a scaling parameter upon the cryoconite mass and respiration fluxes (and their uncertainty) after assuming that respiration rates within the dispersed granules were identical to those measured during the incubations.

3. Results

[19] Table 2 shows the bacterial production and respiration deduced from the in situ incubations. The data show carbon fluxes for the entire habitat, as well as the proportion of total activity that was attributed to the water overlying the cryoconite debris. In all cases, the debris were the dominant part of the system (>90%), producing average bacterial production rates of 0.040 μg C g^{-1} h^{-1} and average respiration rates of 1.17 μg C g^{-1} h^{-1}. These data also show that variability in the respiration rates from site to site was lower than that of the bacterial production, the coefficients of variation being 14 and 50%, respectively.

[20] Figure 5a shows the gridded distribution of total cryoconite (i.e., the sum of cryoconite holes and stream cryoconite cover) in the UAV images, while Figure 5b indicates the proportion of total cryoconite in the UAV images that was found within cryoconite holes. Also shown, but using different symbols, are the ground survey data. All images were found to contain cryoconite, although no patterns in the distribution of cryoconite were evident in either the UAV or the ground-based images. In the case of the more extensive UAV survey, very significant variability was found along the various transects, such that the coefficients of variation were between 48% and 72%. The variability was particularly important where cryoconite cover was greatest, between 226 and 275 m. Here the "patches" of high cryoconite cover (up to 1.4%) coincided with low surface slopes and sometimes strong surface foliation patterns in the glacier ice (250 m). In all these cases (certainly below 300 m) these patches were dominated by stream cryoconite deposits, indicating a relationship between small stream flow paths and structural features upon the glacier surface. However, further up glacier (above 325 m and also west of the glacier center line in the 276–325 elevation interval) the importance of stream deposits dropped markedly to mean values that approached zero.

[21] In all, the UAV images produced an estimate of total cryoconite cover of 0.42% of the glacier surface, equivalent to a dry mass density of 4600 kg km^{-2} of cryoconite debris (Table 1). The ground-based observations indicated a greater proportion of cryoconite cover, the average being 1.23% for all the quadrat sampling sites. The scaling procedure described above therefore resulted in a dry mass density of 10600 kg km^{-2} across the glacier.

4. Discussion

[22] Figure 5a shows that cryoconite is dispersed all over the glacier, with no significant trends along elevation gradients or patterns according to aspect. In fact, the only observable pattern is the tendency for cryoconite holes to

dominate over stream cryoconite in the upper glacier (Figure 5b). This is simply an artefact of the low abundance of streams at higher elevations due to the lower rates of meltwater production there. Down glacier, the proportion of cryoconite within streams increases at the expense of cryoconite holes, testifying to the importance of continuous redistribution by meltwater. The exception is west of the glacier center line in the 276–325 m elevation interval, where shading from nearby mountains, moderate elevation and a small runoff contributing area limit stream development. Otherwise, the apparent significance of meltwater in the continuous redistribution of cryoconite across the glacier ablation area suggests that our data might be best described as a snapshot representative of late summer conditions (i.e., mid-August). At this time, lower solar angles, significant cloud cover and the glacier's northerly aspect will tend to minimize solar heating of the cryoconite debris, making the formation and persistence of stable, deep cryoconite holes far less likely than earlier in the summer. The implication therefore is that far more surveys are required before the temporal dynamics of cryoconite cover upon melting glaciers can be captured.

[23] Despite the above limitation, a very strong elevation control upon the duration of melting conditions (Table 1) means that seasonal microbial activity will vary systematically upon Midtre Lovénbreen, with the shortest periods of activity being found in the steeper, north facing parts of the upper glacier. Table 1 suggests that between 30 and 70 d of cryoconite activity may be typical upon the snow-free parts of the glacier. This produced respiration CO_2 fluxes of 6.3 and 5.1 kg C km^{-2} a^{-1} for the entire glacier during 1998 and 2000, or 14 and 12 kg C km^{-2} a^{-1} if dispersed cryoconite granules were as active (see Table 1). Of this, about 65% was achieved in EIs between 275 and 550 m, reflecting the importance of glacier hypsometry as a control upon total respiration (since 66% of the glacier area is also found between 275 and 550 m).

[24] Greater respiration CO_2 fluxes than those presented above can be expected if bacterial metabolism is significant earlier in the summer: for example when the glacier surface is raised to the melting point and runoff percolation to the base of the snowpack has begun. This is difficult to assess because most cryoconite habitats are initially entombed beneath a superimposed ice layer that can constitute as much as 37% of Midtre Lovénbreen's annual accumulation [*Wright et al.*, 2005]. The sensitivity of the glacier respiration model to this problem was assessed by assuming that the energy requirement for melting to begin in all cryoconite habitats is satisfied following the ablation of a fixed proportion of the winter snow and ice accumulation. Thus if this condition is met following the ablation of 20% of the winter accumulation in each EI, then respiration takes place across a wider range of elevations (i.e., up to 600 m), the duration of activity increases (e.g., an additional 8 d in the 176–225 EI), and the respiration CO_2 flux of the entire glacier rises by 40%. At a threshold equivalent to 50% of winter accumulation, the respiration flux rises by just 19%, taking place in the same number of EIs as that captured in the original model (Table 1). The results therefore suggest that the role of respiration prior to snowpack removal must be assessed before ice masses with a large accumulation area ratio (e.g., the Greenland Ice Sheet) can be considered in the manner presented here. Otherwise, for Midtre Lovénbreen, where ablation rapidly removes snow cover, only modest increases in the total respiration flux are likely to occur when this problem is considered.

4.1. Net Heterotrophy or Autotrophy?

[25] The fluxes presented in Table 1 demonstrate that even supraglacial meltwaters, which interact with all types of cryoconite habitat, can export alkalinity that is derived from the respiration of organic carbon. However, the fate of this CO_2 is unclear, and will remain so until the impact of primary production is considered in some detail. Our respiration fluxes appear to be just 3–9% of the carbon sequestration rates estimated within Midtre Lovénbreen cryoconite holes by *Säwström et al.* [2002], and about 5% of those deduced during the present study using a virtually identical methodology (B. Sattler et al., unpublished data, 2006). This implies that glacier surface ecosystems upon Midtre Lovénbreen are most likely net autotrophic, at least after they have lost their snowpacks. However, both Säwström et al.'s and Sattler et al.'s primary production rates are far more variable than the respiration rates presented here. Further, net heterotrophy, rather than autotrophy, seems most likely early in the summer when microorganisms are buried by a deep, wet snowpack. These two points suggest that we are not yet ready to constrain the net impact of biological activity upon carbon fluxes, and this uncertainty will remain until more studies of the spatial and temporal variability of biological processes rates have been undertaken in a range of supraglacial habitats.

4.2. Activity Versus and Respiration

[26] The bacterial carbon production (BCP) and community respiration (CR) data enabled estimation of the microbial growth efficiency, defined as (BCP/(BCP + CR)). In so doing, we found that the microbial growth efficiency in the water was ~0.35%, which is typical of ultra oligotrophic environments with nutrient limitation. Otherwise, microbial growth efficiency in the debris was about 3.3%, which is still low and typical of oligotrophic conditions, but ~10 times higher that in the water. The fact that the debris appear more typical of nutrient-rich conditions than the overlying water is not surprising because dilute runoff continuously enters the streams and holes during much of the summer. A recent study by *Säwström et al.* [2007] also showed that multiple factors, such as phosphorus, carbon and temperature are responsible for limitation of the bacterial community in Midtre Lovénbreen cryoconite waters. The differences between the waters and the debris also demonstrate the importance of substrate supply for enhanced bacterial activity, a relationship that has been established in a range of glacial habitats [e.g., *Sharp et al.*, 1999; *Hodson et al.*, 2007].

5. Conclusion

[27] Aerial reconnaissance offers great potential for mapping the distribution of active cryoconite habitats upon glaciers and ice sheets worldwide. The data collected also offer a quick basis for scaling up community-scale measurements, such as bacterial activity, respiration and photosynthesis. This paper has demonstrated this potential and reported significant rates of bacterial production (~0.040 μg C g^{-1} h^{-1}) and respiration

($\sim$1.17 μg C g^{-1} h^{-1}) at in situ conditions for the first time. Scaling up across an entire Svalbard glacier produced a total system respiration flux of 5.1–6.3 kg C km^{-2} a^{-1} from larger cryoconite holes and stream cryoconite deposits in streams. However, a problem with our aerial reconnaissance approach is that smaller, dispersed granules of cryoconite (<0.25 cm^2) could not be resolved but are likely to have been active during the melt season. Ground-based photography was therefore undertaken to assess their spatial distribution and mass. We found that on average, the mass distribution of all cryoconite per unit area increases by a factor of 2.31 when these small features are considered. Thus the potential carbon flux from respiration could have been 12–14 kg C km^{-2} a^{-1} for the summers considered. These new data therefore demonstrate for the first time that active microbial habitats upon melting ice surfaces can contribute significantly to carbon cycling in heavily glacierized environments.

[28] **Acknowledgments.** Hodson acknowledges NERC Connect A award; NE/D522189/1, the University of Sheffield Knowledge Transfer Opportunities Funds and an award from the Earth Science Fund. Anesio and Hodson acknowledge NERC Small grant NE/D007321/1. Interaction between Hodson, Sattler, and Anesio was supported via a British Council Austria Research Collaboration award. The authors acknowledge helpful comments from Martyn Tranter, Andrew Fountain, and the Associate Editor.

References

Anesio, A. M., B. Mindl, J. Laybourn-Parry, A. J. Hodson, and B. Sattler (2007), Viral dynamics in cryoconite holes on a high Arctic glacier (Svalbard), *J. Geophys. Res.*, *112*, G04S31, doi:10.1029/2006JG000350.

Bell, R. T. (1993), An explanation for the variability in the conversion factor deriving bacterial cell production from incorporation of [^{3}H]-thymidine, *Limnol. Oceanogr.*, *35*, 910–915.

Hagen, J. O., J. Kohler, K. Melvold, and J. G. Winther (2003), Glaciers in Svalbard: Mass balance, runoff and freshwater flux Polar research, *Pol. Res.*, *22*, 145–159.

Hodson, A. J., P. N. Mumford, J. Kohler, and P. M. Wynn (2005a), The High Arctic glacial ecosystem: New insights from nutrient budgets, *Biogeochemistry*, *72*, 233–256.

Hodson, A. J., J. Kohler, and M. Brinkhaus (2005b), Multi-year water and surface energy budget of a high latitude polythermal glacier: Evidence for over-winter storage in a dynamic subglacial reservoir, *Ann. Glaciol.*, *42*, 42–46.

Hodson, A. J., A. M. Anesio, M. Tranter, A. G. Fountain, A. M. Osborn, J. Priscu, J. Laybourn-Parry, and B. Sattler (2007), Glacial ecosystems, *Ecol. Monogr.*, in press.

Kaštovská, K., J. Elster, M. Stibal, and H. Šantrùèková (2005), Microbial assemblages in soil microbial succession after glacial retreat in Svalbard, *Microbial Ecol.*, *50*, 396–407.

Kirchman, D. L. (2001), Measuring bacterial biomass production and growth rates from leucine incorporation in natural aquatic environments, in *Marine Microbiology*, *Methods Microbiol.*, vol. 30, edited by J. H. Paul, pp. 227–237, Academic, New York.

Mindl, B., A. M. Anesio, K. Meirer, A. J. Hodson, J. Laybourn-Parry, R. Sommaruga, and B. Sattler (2007), Factors influencing bacterial dynamics along a transect from supralgacial runoff to proglacial lakes of a high Arctic glacier, *FEMS Microbial Ecol.*, *59*, 307–317.

Säwström, C., P. N. Mumford, W. Marshall, A. Hodson, and J. Laybourn-Parry (2002), The microbial communities and primary productivity of cryoconite holes in an Arctic glacier (Svalbard, 79°N), *Pol. Biol.*, *25*, 591–596.

Säwström, C., W. Granéli, J. Laybourn-Parry, and A. M. Anesio (2007), High viral infection rates in Antarctic and Arctic bacterioplankton, *Environ. Microbiol.*, *9*, 250–255.

Sharp, M., J. Parkes, B. Cragg, I. J. Fairchild, H. Lamb, and M. Tranter (1999), Bacterial populations at glacier beds and their relationship to rock weathering and carbon cycling, *Geology*, *27*, 107–110.

Smith, D. C., and F. Azam (1992), A simple economical method for measuring bacterial protein synthesis rates in seawater using 3H-leucine1, *Mar. Microbial. Food Webs*, *6*, 107–114.

Takeuchi, N., S. Kohshima, Y. Yoshimura, K. Seko, and K. Fujita (2000), Characteristics of cryoconite holes on a Himalayan glacier, Yala Glacier central Nepal, *Bull. Glaciol. Res.*, *17*, 51–59.

Taylor, J. R. (1982), *An Introduction to Error Analysis: The Study of Uncertainties if Physical Measurements*, Univ. Sci. Books, Herndon, Va.

Tranter, M., A. Fountain, C. Fritsen, B. Lyons, J. Priscu, P. Statham, and K. Welch (2004), Extreme hydrochemical conditions in natural microcosms entombed within Antarctic ice, *Hydrol. Processes*, *18*, 379–387.

Wright, A., J. Wadham, M. Siegert, A. Luckman, and J. Kohler (2005), Modelling the impact of superimposed ice on the mass balance of an Arctic glacier under scenarios of future climate change, *Ann. Glaciol.*, *42*, 277–283.

A. M. Anesio, Bristol Glaciology Centre, School of Geographical Sciences, University of Bristol, Bristol BS8 1SS, UK.

C. Clark, A. Dye, A. Hodson, T. Irvine-Fynn, F. Ng, and J. Quirk, Department of Geography, University of Sheffield, Sheffield S10 2TN, UK. (a.j.hodson@sheffield.ac.uk)

J. Kohler, Norsk Polarinstitutt, Polar Environmental Center, N-9296 Tromsø, Norway.

P. McCloy and R. Watson, HighSpy, Beckets, Red House Lane, Elstead, GU8 6DS.

B. Sattler, Institute of Ecology, University of Innsbruck, Technikerstraße 25, A-6020, Innsbruck, Austria.